



Improved forest change detection with terrain illumination corrected Landsat images



Bin Tan^{a,b,*}, Jeffrey G. Masek^b, Robert Wolfe^b, Feng Gao^c, Chengquan Huang^d, Eric F. Vermote^d, Joseph O. Sexton^{d,f}, Greg Ederer^{b,e}

^a Earth Resources Technology, Inc., Laurel, MD, 20707, United States

^b NASA Goddard Space Flight Center, Greenbelt, MD 20771, United States

^c USDA-ARS Hydrology & Remote Sensing Lab, Beltsville, MD 20705, United States

^d Department of Geography, University of Maryland, College Park, MD 20742, United States

^e Sigma Space Corp., Lanham, MD 20706, United States

^f Global Land Cover Facility, University of Maryland, College Park, MD 20742, United States

ARTICLE INFO

Article history:

Received 24 May 2012

Received in revised form 17 May 2013

Accepted 19 May 2013

Available online 22 June 2013

Keywords:

Illumination correction

Topographic effect

Landsat

LEDAPS

TDA-SVM

ABSTRACT

An illumination correction algorithm has been developed to improve the accuracy of forest change detection from Landsat-derived reflectance data. This algorithm is based on an empirical rotation model and was tested on Landsat image pairs over the Cherokee National Forest, Tennessee; Uinta–Wasatch–Cache National Forest, Utah; San Juan National Forest, Colorado; and Sinkyone Wilderness State Park, California. The illumination correction process successfully eliminated correlation between Landsat reflectance and illumination condition. Comparison to forest-change maps derived from uncorrected images showed significant disagreement, ranging from 23% to 45%. Validated against high-resolution (1 m or less) time-serial images, the illumination correction decreased overestimation of forest gains and losses and improved specificity in detection of major forest changes. The overall accuracy increases 34% at the Cherokee Forest site and about 10% at the other three sites. The disagreement rate between change maps from the original and corrected Landsat images increased with increasing terrain inclination angle, with the relationship between illumination condition and the disagreement rate following a V-shaped curve that varied among sites. The lowest disagreement rate occurred when illumination condition was slightly smaller than that of a horizontal field. The correction for topographic illumination should be considered as a standard pre-processing step for land cover classification and land use change detection, especially for mountainous areas.

© 2013 Elsevier Inc. All rights reserved.

1. Introduction

Landsat imagery is widely used to monitor changes in land surface conditions, including changes in forest cover, which impact Earth's energy balance, carbon cycle, water cycle and biogeochemical processes (Band, 1993; Huang et al., 2008; Pandey, 2002). To quantify such changes, two Landsat images acquired before and after the forest change are typically examined by visual interpretation or automated analysis. With the Landsat archive becoming freely available, the main challenge for generating continental or global forest change maps at Landsat resolution (30 m) is an effective and accurate change detection algorithm (Huang et al., 2008). Various computer based change-detection algorithms have been developed (Foody & Mathur, 2004; Huang et al., 2010a, 2010b; Masek et al., 2008; Townshend et al.,

2012). The key process in these algorithms is the spectral analysis of a set of training pixels and discriminating appropriate spectral thresholds that can be applied to the whole image scene or multiple scenes to define the area of forest change.

One important assumption underlying these algorithms is that the spectral characteristics of the training pixels represent those of the forest pixels within the study region. However, topographic illumination effects (shadow, slope, etc.) negate this assumption. Varying illumination conditions due to topography lead to significant changes in the observed spectral characteristics of a group of neighboring pixels, even in the absence of variations in land cover type or condition. Therefore, illumination correction, also known as topographic correction or topographic normalization, is an important step in pre-processing high-resolution remote sensing data for forest change detection studies. Illumination correction refers to the compensation for solar irradiance to minimize the variability of observed reflectance for similar targets due to topography and Bidirectional Reflectance Distribution Function (BRDF) effects.

* Corresponding author at: Code 619, NASA GSFC, Greenbelt, MD 20707, United States. Tel.: +1 3016145965.

E-mail address: bin.tan@nasa.gov (B. Tan).

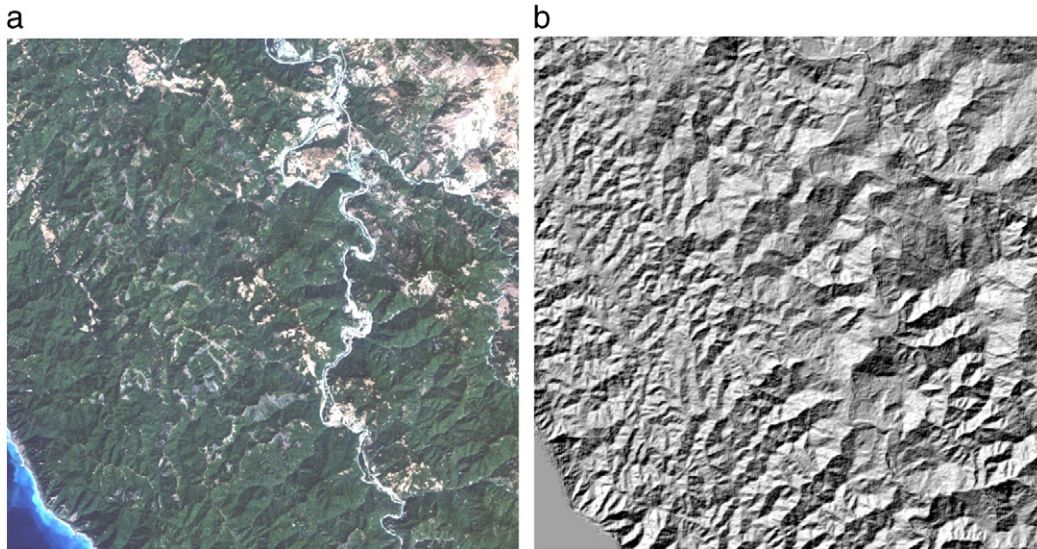


Fig. 1. A sample Landsat image (a) and the corresponding illumination condition (IC) map (b). The Landsat image is the top-of-atmosphere reflectance. The IC map is calculated from digital elevation map (DEM), the solar zenith and azimuth angles.

There are several existing illumination correction models for Landsat images (Ekstrand, 1996; Meyer et al., 1993; Riano et al., 2003; Shephard & Dymond, 2003; Teillet et al., 1982; Vicente-Serrano et al., 2008). However, these models tend to over-correct over shallowly illuminated slopes (Holben & Justice, 1980; Meyer et al., 1993). The goal of this study was to produce illumination-corrected Landsat-TM data with the quality needed for more accurate forest change detection (Masek et al., 2007, 2008) in the Landsat Ecosystem Disturbance Analysis Adaptive Processing System (LEDAPS) (Masek et al., 2006; Wolfe et al., 2004). In this paper, we introduce an empirically based rotation-correction model, and apply it to correct Landsat images in four study sites spanning a range of topographic and forest-structural conditions. To assess the improvements in change-detection accuracy, the forest change maps were validated against high-resolution imagery and their accuracies were compared to those of change maps derived from uncorrected Landsat data.

2. Methods

2.1. Algorithm

2.1.1. Terrain illumination correction model

The relative solar incidence angle, or illumination condition (IC), is the basis of all correction models for compensating reflectance. IC is defined as:

$$IC = \cos(Z) \cos(S) + \sin(Z) \sin(S) \cos(\varphi_z - \varphi_s) \quad (1)$$

where Z is the solar zenith angle, S is the topographic slope angle ($0 =$ horizontal). φ_z is the solar azimuth angle, and φ_s is the aspect angle of the topographic surface ($0 =$ north). IC ranges from -1 (minimum illumination) to 1 (maximum illumination). For a horizontal surface, $IC = \cos(Z)$. A sample Landsat image and the corresponding IC image are shown in Fig. 1.

Two illumination corrections models are widely used (Teillet et al., 1982). The first is the cosine model:

$$L_H = L_I \left(\frac{\cos(Z)}{IC} \right) \quad (2)$$

where L_H is the corrected reflectance (for a horizontal surface) and L_I is the observed reflectance on the incline surface. This cosine model assumes a Lambertian surface, and is wavelength-independent.

The second common approach is the C model:

$$L_H(\lambda) = L_I(\lambda) \frac{\cos(Z) + c(\lambda)}{IC + c(\lambda)} \quad (3)$$

where λ represents a specific wavelength. Any variable followed by (λ) is a wavelength-dependent variable. The variable c is a wavelength-dependent adjustment coefficient; $c = b / a$, where b and a are the intercept and slope of the linear regression for a specific wavelength:

$$L_I(\lambda) = a(\lambda) \cdot IC + b(\lambda). \quad (4)$$

The C model does not assume a Lambertian surface and is wavelength-dependent. Several studies have reported that the cosine model overcorrects surface reflectance, especially in low IC regions (Duguay & LeDrew, 1992; Meyer et al., 1993; Riano et al., 2003). Overcorrection here implies that dark slopes with low illumination can become unnaturally bright following application of the model. The C model can avoid the overcorrection to some degree, although it remains a significant issue in some low IC regions. Both methods perform better in the near-infrared band than the visible bands.

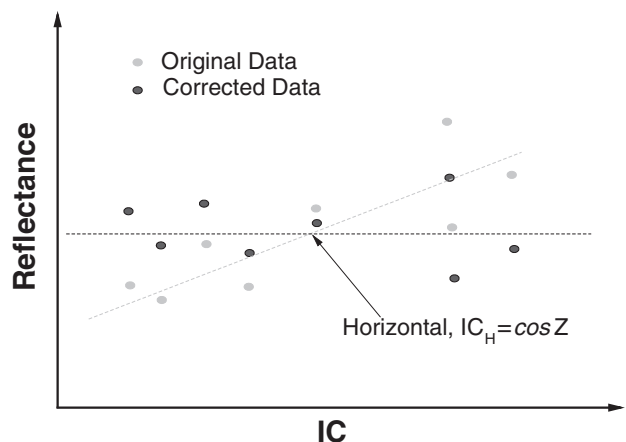


Fig. 2. A schematic diagram illustrating the empirical rotation model. Z is the sun zenith angle.

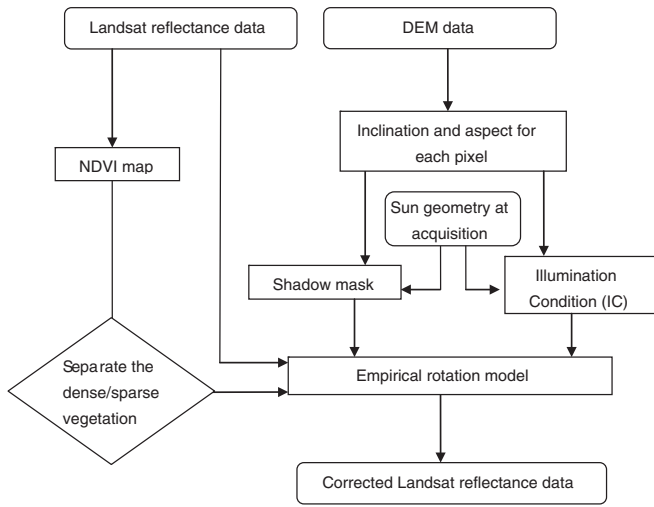


Fig. 3. Data flow and processes of the illumination correction algorithm.

Tan et al. (2010) introduced an empirical rotation model that does not assume a Lambertian surface:

$$L_H(\lambda) = L_l(\lambda) - a(\lambda) * (IC - IC_H) \tag{5}$$

where a is from Eq. (4), and IC_H is the IC for a horizontal surface. IC_H equals the cosine of the solar zenith angle.

This empirical rotation model removes the dependency of the reflectance on IC according to the linear relationship presented in Eq. (4) (Fig. 2). Tan et al. (2010) compared this model with cosine and C models. It was found that the rotation model performance

consistently well on both top-of-atmosphere and top-of-canopy Landsat reflectance data. In this study, this model is used as the core model of the illumination correction algorithm.

2.1.2. Shadow removal through ray tracing algorithm

“Hard shadow” regions are illuminated by diffuse solar radiation only. The absence of direct solar radiation voids the assumption of the relationship between reflectance and IC presented by Eq. (4). Therefore, pure shadow pixels should be excluded (masked) when calculating the linear relationship. They should also be avoided when applying illumination correction. There are two types of shadow pixels: self-shadowed pixels, which have aspect angles oriented away from the sun (where $IC < 0$), and cast-shadowed pixels, which are oriented towards the direction of the sun but sunlight is blocked by other interceding objects such as mountains. The first type of shadow pixels were excluded by simply examining IC values. For the second type of shadow pixels, we used a ray-tracing algorithm to identify them. The track of a ray from the center of a pixel to the sun is calculated (Whitted, 1979); if any other pixels block this ray, this pixel is marked as a cast-shadowed pixel. Otherwise, this pixel is considered as a shadow-free pixel.

2.1.3. Full illumination correction algorithm

The relationship between surface reflectance and IC depends on the vegetation type (for vegetated landcover) or soil/rock type (for non-vegetated landcover). However, there are no such fine-resolution (≤ 30 m), detailed land cover maps at continental or global extents. Considering the context of this study is to detect forest and non-forest, a rough separation of dense and sparse vegetation is sufficient, which we perform using a threshold of 0.5 Normalized Difference Vegetation Index (NDVI). In a 3-km by 3-km moving window, two linear

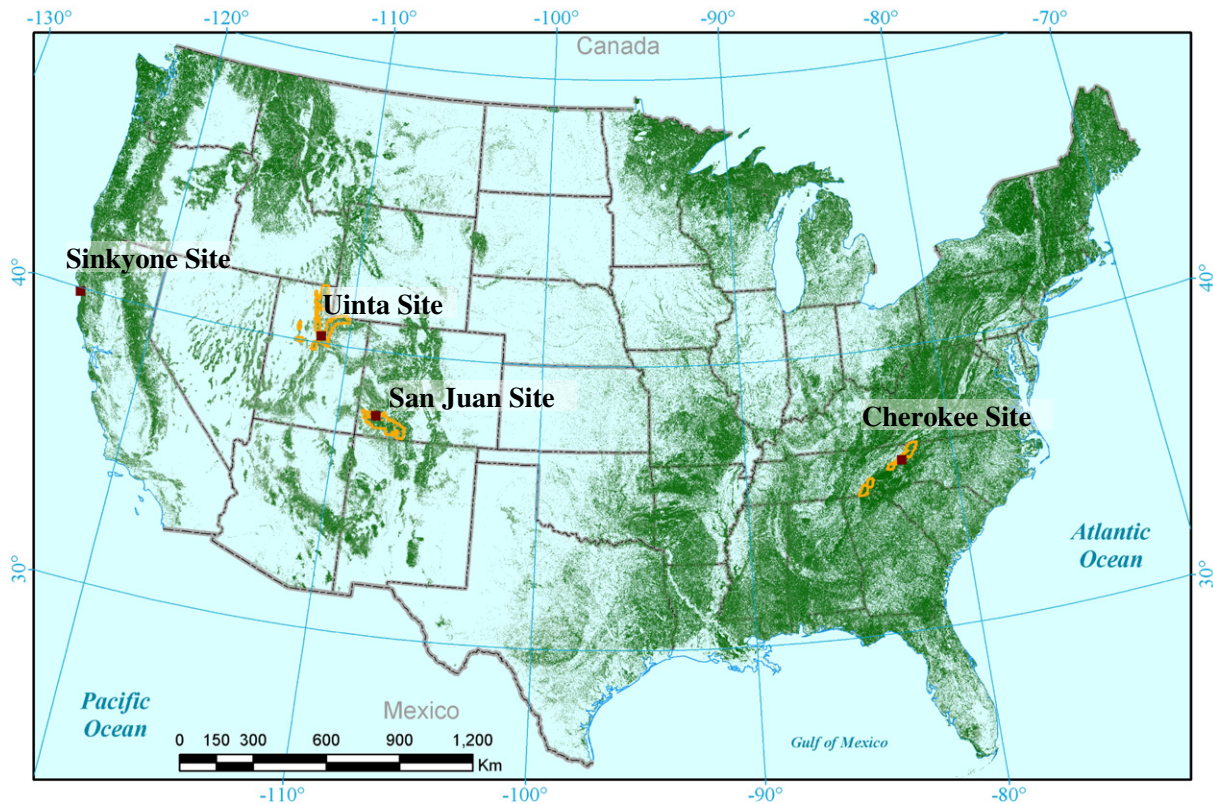


Fig. 4. The locations of four study sites (red rectangles) and the administrative boundaries (orange lines) for the national forests and the state park where the study sites are located. The three national forests are Cherokee, Uinta–Wasatch–Cache, and San Juan National Forests. One state park is the Sinkyone Wildness State Park. The detailed information of the four study sites is in Table 1.

Table 1
Overview of four study sites. SD is the abbreviation of standard deviation.

Name	Site center location	WRS path/row	State	Landsat imagery acquisition date	Primary forest type	Orientation (degrees)		Slope (degrees)		IC	
						Mean	SD	Mean	SD	Mean	SD
Cherokee National Forest	36.057 N, 82.475 W	18/35	Tennessee	1995-10-18 2001-10-26	Deciduous broadleaf forest	191.4	107.1	11.2	6.3	0.55	0.14
Sinkyone Wilderness State Park	39.877 N, 123.898 W	46/32	California	1995-08-19 2004-09-04 2003-05-13	Evergreen needleleaf forest	183.2	103.1	12.8	5.8	0.72	0.11
Uinta–Wasatch–Cache National Forest	40.251 N, 111.405 W	37/32	Utah	1989-07-04 2000-09-12	Evergreen needleleaf forest	181.3	102.0	13.0	7.0	0.84	0.10
San Juan National Forest	37.757 N, 108.110 W	35/34	Colorado	1989-07-02 2000-06-06	Evergreen needleleaf forest	198.0	101.8	12.3	7.4	0.84	0.09
										0.75	0.12

relationships, one for the dense vegetation and the other for the sparse vegetation, are retrieved.

Fig. 3 presents the data flow of the illumination correction algorithm. There are two major input data sets, Landsat reflectance data and DEM data, and one ancillary value, the solar geometry when the Landsat data was acquired. The NDVI map is retrieved from the

Landsat reflectance data. The average inclination and aspect for each pixel are calculated from the DEM data. This information, combined with the solar geometry, is used to produce the shadow mask and calculate IC. The Landsat reflectance data, the NDVI map, the shadow mask, and the IC are the inputs to the core model. The NDVI map is used to separate dense and sparse vegetation pixels. The pixels

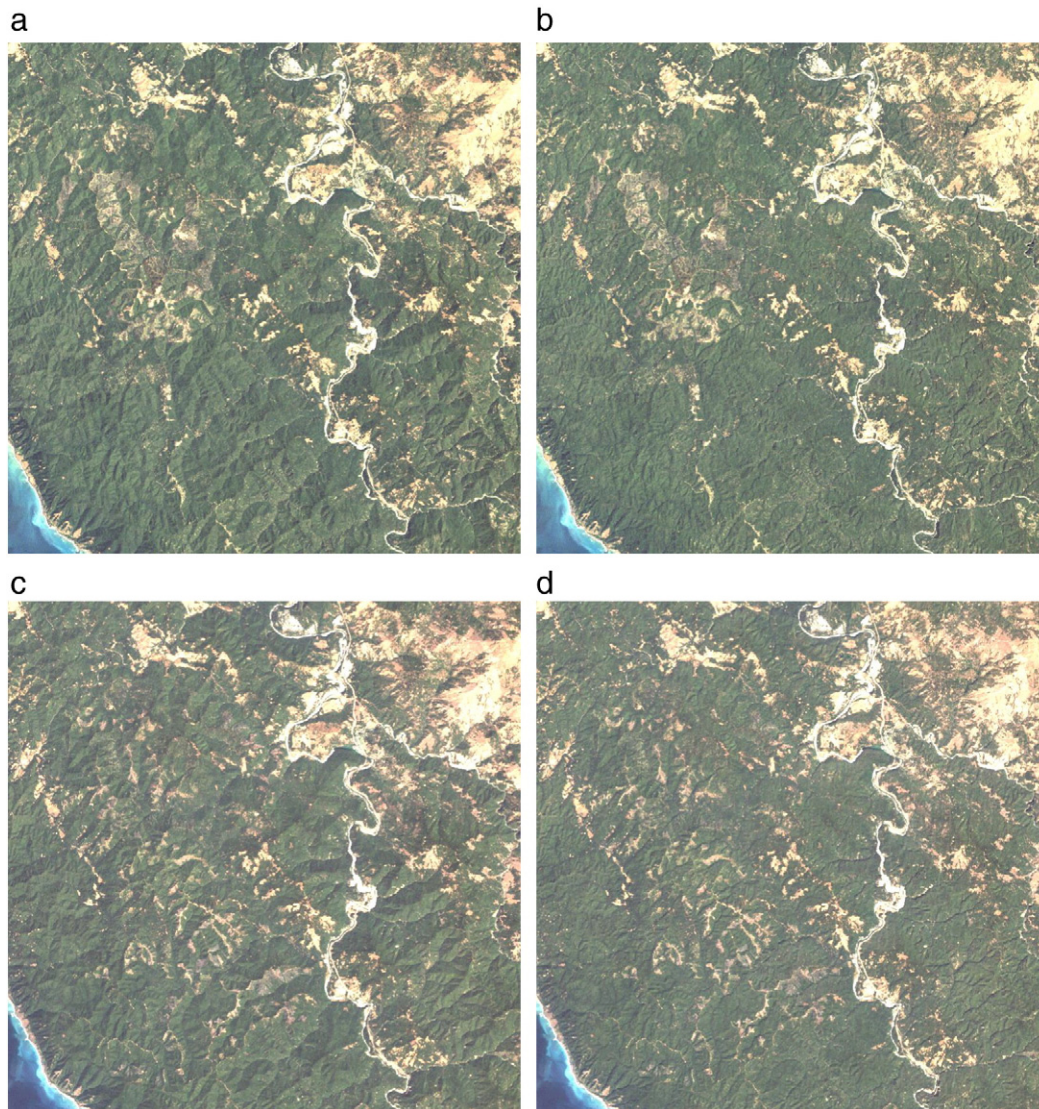


Fig. 5. The validation site within Sinkyone Wilderness State Park (WRS path 46 row 32). The panels a and b are original and corrected Landsat images, respectively, acquired on 1995-08-19. The panels c and d show original and corrected images acquired on 2004-09-04. The images are true color images, whose RGB combination is Landsat bands 3, 2 and 1. It should be noted that some minor topographic effects are not corrected due to the limited resolution of the DEM data.

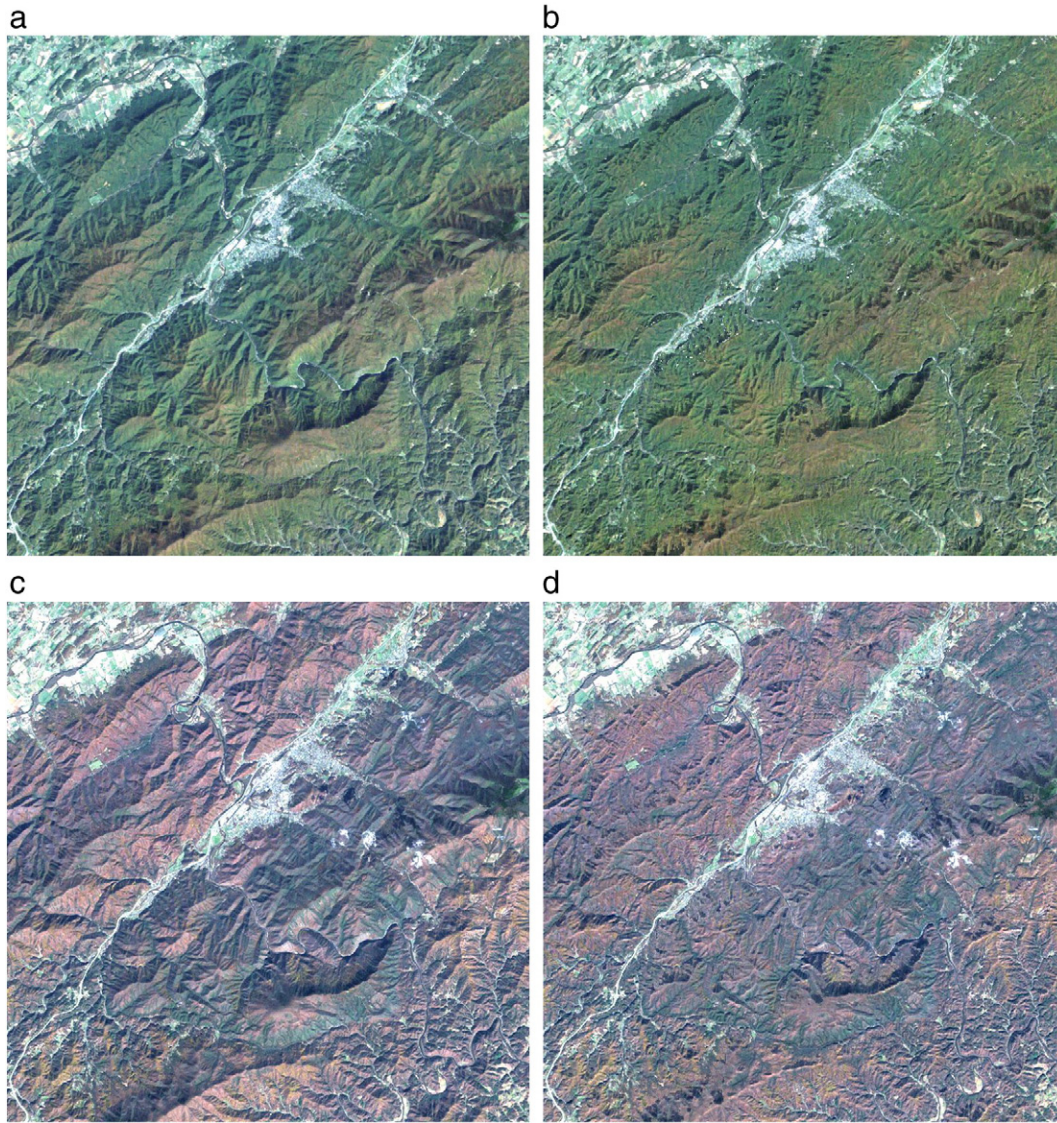


Fig. 6. The validation site within Cherokee National Forest (WRS path 018 row 035). The panels a and b are original and corrected Landsat images respectively acquired on 1995-10-18. The panels c and d, original and corrected Landsat images respectively, were acquired on 2001-10-26. The images are true color images, whose RGB combination is Landsat bands 3, 2 and 1.

identified in the shadow mask are excluded from the processing. The core model then processes the Landsat reflectance data and the IC map and generates the illumination-corrected Landsat reflectance data. Ideally this corrected reflectance is equivalent to the reflectance that would be seen for a horizontal surface and identical vegetation conditions.

2.2. Study sites

Four study sites within the United States were selected: the Cherokee, Uinta–Wasatch–Cache, and San Juan National Forests and the Sinkyone Wilderness State Park (Fig. 4). The Cherokee National Forest, located in the southern Appalachian Mountains of east Tennessee, is forested with a mix of mesic temperate evergreen and deciduous tree species, with deciduous hardwood species dominating on warmer, drier slopes and evergreen conifers dominating at high elevations and in sheltered coves (Yoke & Rennie, 1996). The Uinta–Wasatch–Cache and San Juan National Forests, located respectively in the Rocky Mountains of northern Utah and southwestern Colorado,

span similar gradient from semi-arid shrub lands and annual grasslands at low elevations and southerly slopes, through taller shrubs and semi-arid mixed forests (primary evergreen conifers, but with large patches of deciduous quaking aspen (*Populus tremuloides*, Michx.)) to alpine tundra and bare rock at the highest elevations (Develice et al., 1986; Floyd-Hanna et al., 1996; Mauk & Henderson, 1984). The Sinkyone Wilderness State Park is located in the King Range on the northern coast of California. This region is characterized by steep slopes that are densely forested with evergreen conifers in sheltered coves and on western slopes influenced by maritime fog and by sparser evergreen oak woodlands on drier inland slopes. Due to their greater isolation, flatter terraces are dominated by grasses and shrubs (Bowcutt, 1996).

All four study sites have steep terrain (Table 1). The sites were selected to represent different forest types and different topographic situations: whereas terrain has comparatively little effect on forest cover (and therefore reflectance) in the Cherokee study area, terrain plays a much greater role in the forest composition of the other three study areas. Due to their aridity and large elevation gradients,

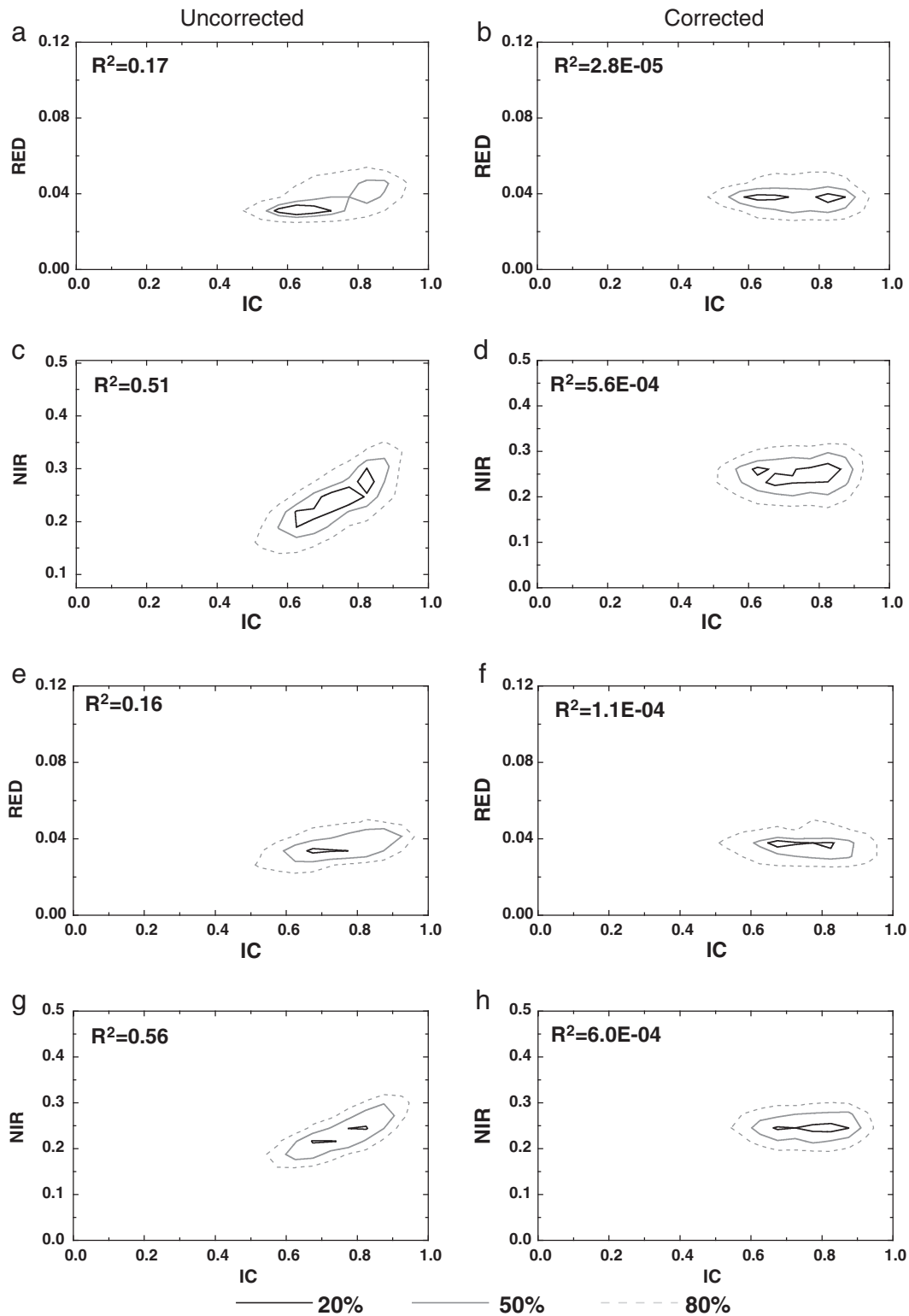


Fig. 7. Data density contour of red and NIR reflectance in reflectance-IC space over the Sinkyo site. The left column is from the original Landsat reflectance, and the right column is from the illumination-corrected Landsat reflectance. The upper four panels are from the Landsat image acquired on 1995-08-19. The lower four panels are from the Landsat image acquired on 2004-09-04. The space enclosed by the black solid line contains 20% data, and the gray solid and light gray dashed lines correspond to 50% and 80% density, respectively.

the Uinta and San Juan study areas are likely to exhibit an indirect effect of terrain on reflectance—through forest composition—in addition to the effect of terrain on reflectance directly. Sinkyo will also likely exhibit this effect, as well as a longitudinal gradient from west

to east correlating to the maritime influence reflectance through forest composition. All sites are within the nominal frame of one Landsat image as defined by the tiling system of the World Reference System (WRS). Each site spans a 24 km by 24 km region (Fig. 4).

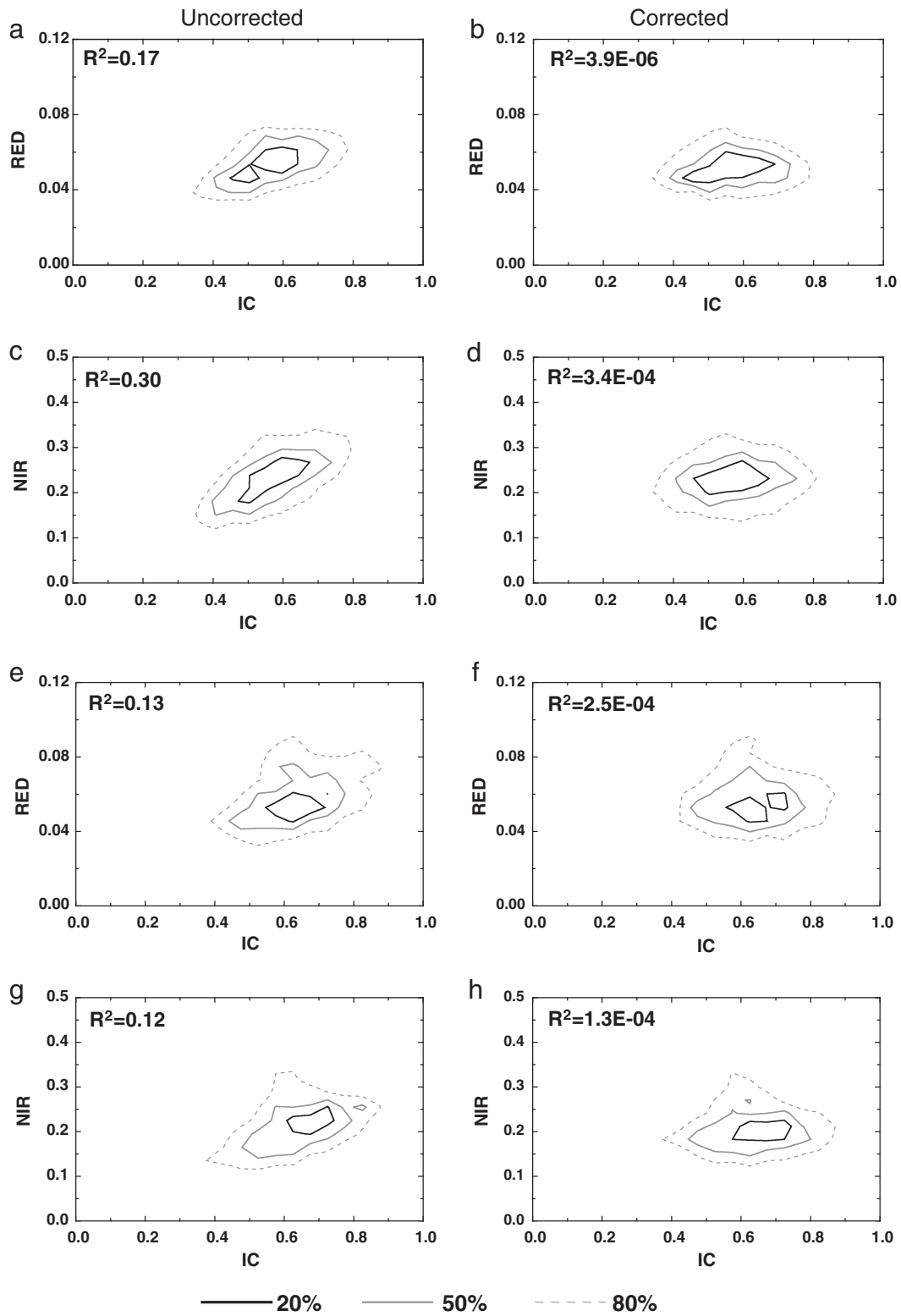


Fig. 8. Data density contour of red and NIR reflectance in reflectance-IC space over the Cherokee site. The left column is from the original Landsat reflectance, and the right column is from the illumination corrected Landsat reflectance. The upper four panels are from the Landsat image acquired on 1995-10-18. The lower four panels are from the Landsat image acquired on 2001-10-26. The space enclosed by the black solid line contains 20% data, and the gray solid and light gray dashed lines correspond to 50% and 80% densities, respectively.

2.3. Data

2.3.1. Landsat imagery

Four Landsat image pairs—one pair for each site—were selected and converted to top-of-canopy reflectance using the 6S model (Vermeote

et al., 1997). Images acquired before 2000 were from Thematic Mapper (TM) and those after 2000 from Enhanced Thematic Mapper Plus (ETM+) (Table 1). Both images from each pair were acquired during the growing season and were as close to the same day of year as possible. The growing season images are helpful to distinguish forest from other

land cover types. The close acquisition times of year are to minimize the phenology state shift. However, when two images were acquired during periods of rapid phenological change, e.g. greenup or senescence, the phenological state shift could be significant even though the two acquisition times of year are very close. Such an example is given later in this paper. The second criterion is to select the images with minimal cloud cover. The cloud either totally blocks satellite observations to the ground (thick cloud) or changes observed spectral characters of the ground (thin cloud). One additional image over Sinkyone site acquired on May 13, 2003 was used to assess the performance of the algorithm when the incident angles of a pair of images vary significantly.

2.3.2. Digital elevation model (DEM)

DEM data are the key input to the illumination correction algorithm. The DEM dataset is used to generate the slope and the illumination condition (IC) map, as well as the topographic shadow mask. The DEM data applied in this study is the Advanced Spaceborne Thermal Emission and Reflection Radiometer (ASTER) Global Digital Elevation Model Version 2 (GDEM V2). The spatial resolution of this data set is 30 m. Sadeq et al. (2012) assessed the accuracy of GDEM-V2 data. They concluded

that the accuracy of ASTER GDEM-V2 is within the accuracy specification (17 m) and without any negative bias which was found in ASTER GDEM-V1 data (Sadeq et al., 2012). Such precision is sufficient for this study.

2.4. Forest change detection algorithm

The forest change detection algorithm applied in this study was an automatic multi-temporal classification method, which consists of Training Data Automation (TDA) procedure and an advanced Support Vector Machines (SVM) algorithm. The TDA procedure automatically selects forest pixels in the input Landsat images and then uses these pixels to train the SVM classifier.

SVM (Borges, 1998; Huang et al., 2002, 2008) is a group of advanced machine learning algorithms that have been increased use in land cover studies (Zhu & Blumberg, 2002). The advantage of SVM algorithm is that it not only simply finds a solution to the land cover classification problem but also provides an optimal solution. The TDA-SVM algorithm has been assessed over 19 forest regions and achieved satisfactory results.

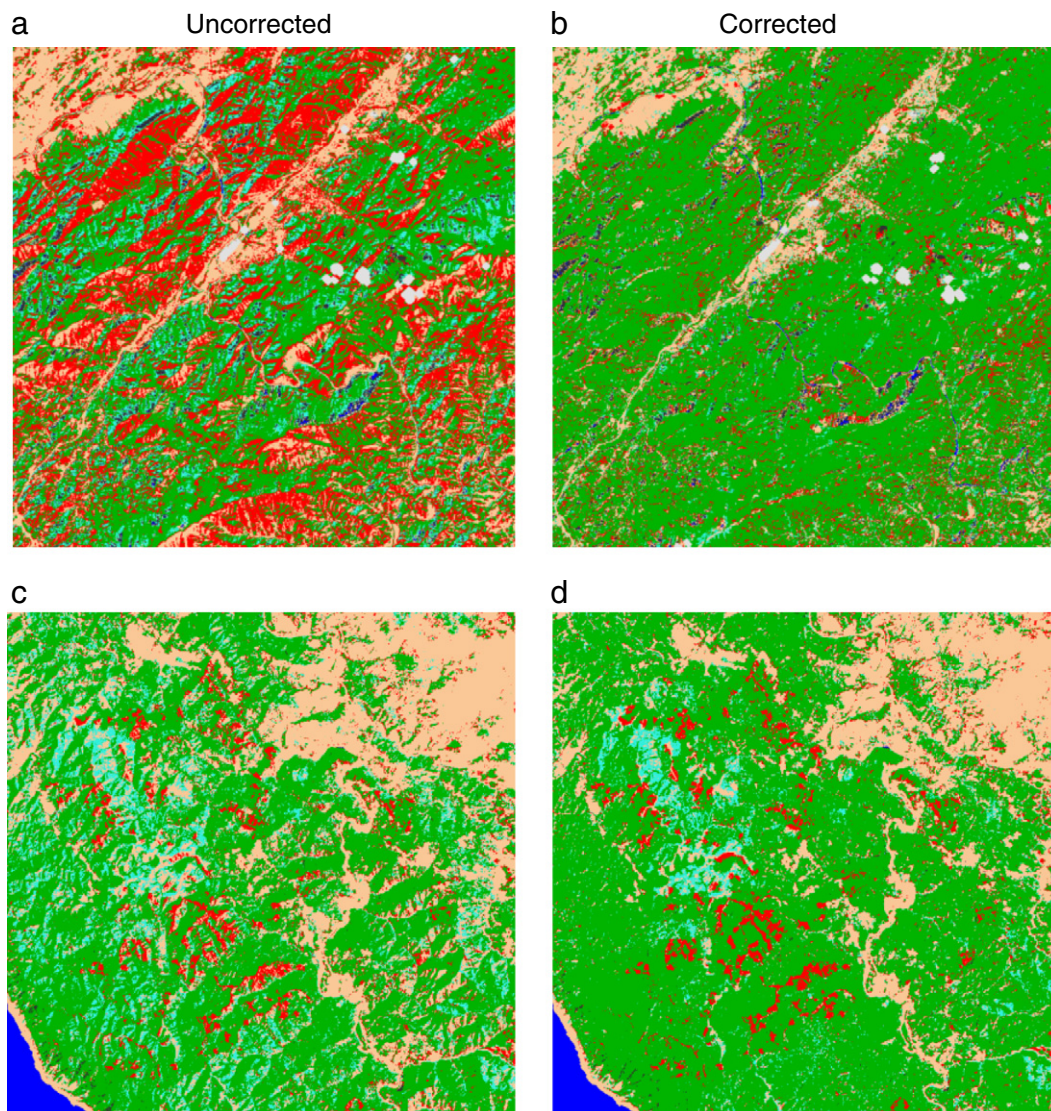


Fig. 9. Forest change maps from original (left) and illumination corrected (right) Landsat image pairs over four study sites: (a) Cherokee, (b) Sinkyone, (c) Uinta, and (d) San Juan.

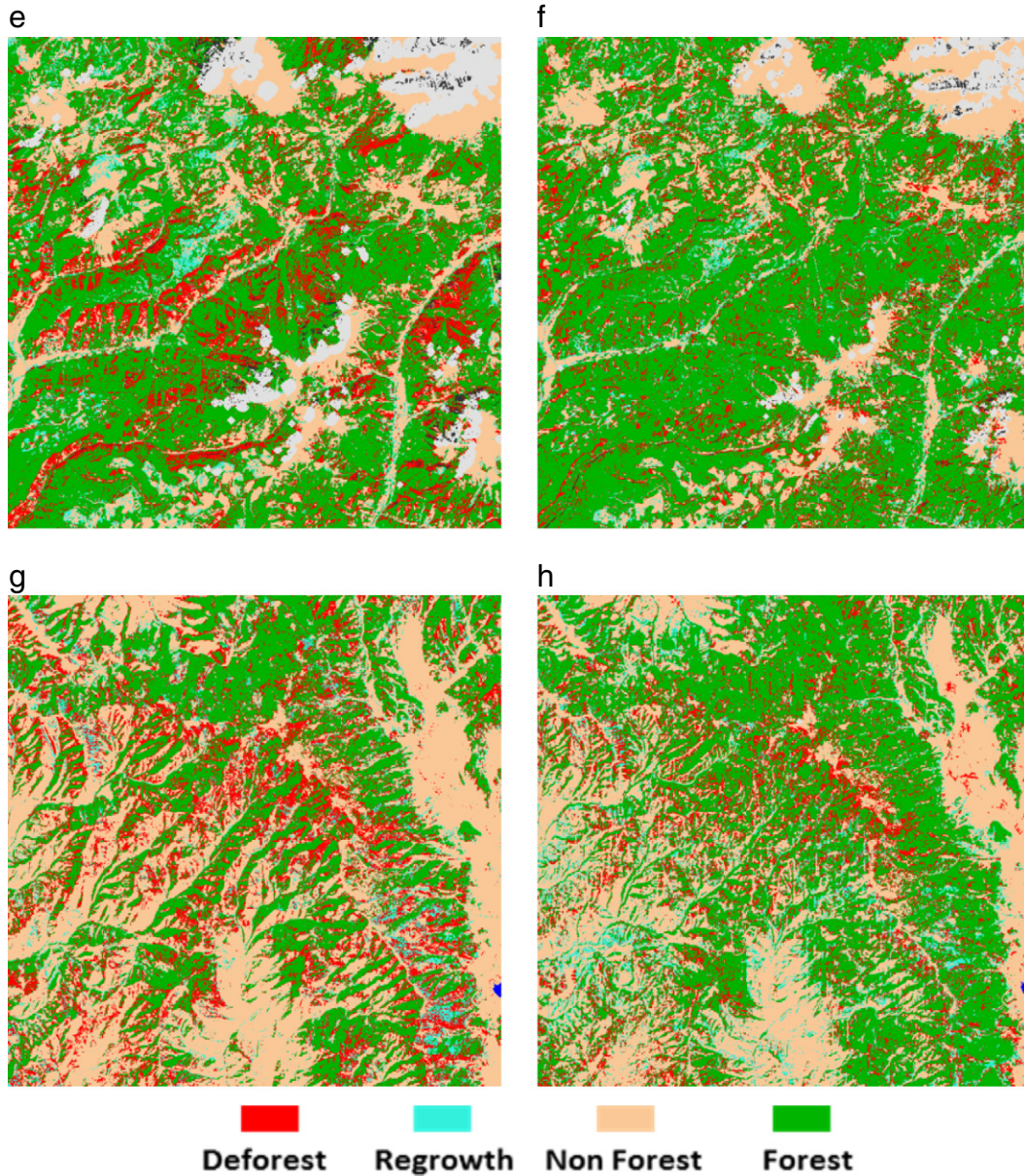


Fig. 9 (continued).

2.5. Algorithm assessment

We assessed the accuracy of forest change detection results from the illumination corrected and original Landsat imagery pairs by visual inspection. For each 24 × 24-km study site, 441 evenly distributed sample points were selected with a spacing of 1.2 km. For each point, the original and corrected Landsat image pairs were inspected visually

alongside high-resolution, time-serial imagery from Google Earth and TerraServer (<http://terraserver.com>). To minimize the impact of possible sub-pixel misregistration, we moved sample points near patch edges toward the patch interior at least 1 pixel away from the edge as determined from the classified map. We also checked the time series reference maps to avoid errors due to the phenology.

Table 2
Confusion Matrix for forest change maps on the Cherokee site (WRS p018r035). Results from original and corrected Landsat data are separated by “\”.

SVM result	Reference data					User's acc
	Forest	Non-forest	Deforest	Regrowth	n	
Forest	41.6\74.2	0.0\0.0	0.2\0.5	0.0\0.0	180\321	99.4\99.4
Non-forest	7.0\2.3	12.6\13.0	0.7\0.0	0.5\0.0	89\66	60.7\84.9
Deforest	26.3\3.7	1.2\0.9	2.6\3.5	0.0\0.0	129\35	8.5\42.9
Regrowth	6.7\0.9	0.5\0.2	0.0\0.0	0.2\0.7	32\8	3.1\37.5
n	351\351	61\61	15\15	3\3		
Producer's acc	51.0\91.4	88.5\91.8	73.3\88.2	33.3\100		Overall 57.0\91.4

Table 3
Confusion Matrix for forest change maps on the Sinkyo site (WRS p046r032). Results from original and corrected Landsat data are separated by “\”.

SVM result	Reference data					User's acc
	Forest	Non-forest	Deforest	Regrowth	n	
Forest	54.7\64.0	0.2\0.0	0.2\0.0	0.0\0.0	231\268	99.1\100.0
Non-forest	4.3\0.5	21.0\20.8	1.2\0.2	0.5\0.0	113\90	77.9\97.8
Deforest	1.4\2.9	0.2\0.2	5.0\5.7	0.0\0.0	28\37	75.0\64.9
Regrowth	7.2\1.0	0.0\0.2	0.0\0.0	4.1\4.8	47\24	36.2\83.3
n	283\286	90\88	27\25	19\20		
Producer's acc	80.9\93.7	97.8\98.9	77.8\96.0	89.5\100		Overall 84.7\95.2

Table 4

Confusion Matrix for forest change maps on the Uinta site (WRS p037r032). Results from original and corrected Landsat data are separated by “\”.

SVM result	Reference data				n	User's acc
	Forest	Non-forest	Deforest	Regrowth		
Forest	38.7\46.8	0.2\1.2	0.0\0.0	0.2\0.0	170\208	98.8\97.6
Non-forest	1.6\0.7	43.1\43.3	0.0\0.5	0.0\0.0	194\193	96.4\97.4
Deforest	9.0\1.2	2.1\1.6	1.6\1.6	0.0\0.0	55\17	12.7\41.2
Regrowth	3.2\2.1	0.0\0.9	0.0\0.0	0.2\0.7	15\16	6.7\18.8
n	228\220	197\202	7\9	2\3		
Producer's acc	73.7\92.3	94.9\93.1	100.0\77.8	50.0\100.0		Overall 83.6\92.4

A confusion matrix was generated for each study site to present the omission error, commission error, and overall accuracy (Stehman and Czaplewski, 1998). In addition, the kappa coefficient, which measures overall agreement between reference data and the forest change maps relative to random allocation of class labels across the sample, was used to assess the algorithm performance. Kappa is often considered as a better indicator because chance agreement is excluded from its calculation (Congalton & Mead, 1983; Huang et al., 2010a, 2010b).

4. Results and discussion

4.1. Illumination-corrected Landsat maps

When selecting the Landsat imagery pair during the growing season, one important criterion is that the acquisition times of year should be very close to minimize the impact of phenology. Fig. 5 shows the original Landsat images (panels a and c) and illumination-corrected Landsat images (panels b and d) over the Sinkyone site (WRS path 46 row 32). These Landsat images were acquired at the peak of growing season, as were those for two other study scenes (Uinta and San Juan sites). However, for the Cherokee site (WRS path 18 row 35), the phenological state shifted significantly despite the small time difference (eight-day) between acquisitions. We kept both situations presented by Figs. 5 and 6 in this study to examine the sensitivity of forest change detection results to phenology state shift in the input Landsat imagery pair.

From Figs. 5 and 6, it can be visually verified that the illumination correction algorithm removed the topographic illumination effect. Figs. 7 and 8 show the data density contour of red and near-infrared (NIR) reflectance in reflectance-IC space over imagery pairs of the Sinkyone and Cherokee sites (imagery pairs shown in Figs. 5 and 6). In the original Landsat images, the uncorrected NIR band generally had the strongest correlation with IC. The strength of the linear relationship (R^2) between red reflectance and IC ranged from 0.1 to 0.2 and from 0.3 to 0.6 for NIR reflectance and IC. An exception is Fig. 8g, which is derived from Fig. 6c, in which the tree leaves were starting to senesce. The correlation between IC and NIR reflectance was only 0.12. The lower correlation for the red band is due to smaller reflectance rate and a more significant atmospheric scattering effect on red than

Table 5

Confusion Matrix for forest change maps on the San Juan site (WRS p035r034). Results from original and corrected Landsat data are separated by “\”.

SVM result	Reference data				n	User's acc
	Forest	Non-forest	Deforest	Regrowth		
Forest	53.2\64.8	0.0\0.0	0.0\0.0	0.0\0.0	210\256	100.0\100.0
Non-forest	2.0\0.0	30.1\29.6	0.0\0.0	0.0\0.0	127\117	93.7\100.0
Deforest	11.9\2.3	0.3\0.3	1.5\2.0	0.0\0.0	54\18	11.1\44.4
Regrowth	0.8\0.3	0.0\0.3	0.0\0.0	0.3\0.5	4\4	25.0\50.0
n	268\266	120\119	6\8	1\2		
Producer's acc	78.4\96.2	99.2\98.3	100.0\100.0	100.0\100.0		Overall 85.1\97.0

NIR reflectance. In the corrected images, the correlations between the red/NIR band and IC are eliminated, where R^2 were smaller than 0.001.

4.2. Improvement on change detection results

Large differences were evident between change maps from uncorrected and corrected reflectances (Fig. 9). There are 45% (29%, 34%, and 23%) area of the Cherokee (San Juan, Uinta, Sinkyone) site has different change detection results after applying illumination correction. Less forest loss was mapped over the Cherokee, Uinta, and San Juan sites and less regrowth over the Sinkyone site when topographically corrected Landsat data were used.

The confusion matrices for the four sites are given in Tables 2–5. Overall accuracy increased the most in the Cherokee site, from 57% to 91%, whereas for the Uinta, San Juan, and Sinkyone sites overall accuracies increased from 84%, 85%, and 85% to 92%, 97%, and 95% respectively. The kappa coefficients of the change detection maps from the original Landsat data were 0.30, 0.72, 0.72, and 0.73 for the Cherokee, Uinta, San Juan and Sinkyone sites. After illumination correction, the kappa coefficients increased to 0.77, 0.86, 0.94, and 0.91 respectively.

A large amount of persistent (no-change) forest was misclassified as non-forest, forest loss, or regrowth. In the change maps from original Landsat imagery pairs, misclassified forest pixels ranged from 18% (Sinkyone) to 49% (Cherokee). After illumination correction, this range dropped to 4% (San Juan) to 9% (Cherokee). The accuracy of forest-loss and regrowth classes regrowth increased especially after illumination correction. The average user's accuracy of forest loss (regrowth) increased from 27% (18%) to 48% (47%). The average producer's accuracy of forest loss (regrowth) increased from 88% (68%) to 91% (100%). The high producer's accuracy indicates that the classification results captured almost all actual forest changes. However, the relatively low user's accuracy suggests that some of the changes presented by the change detection results were actually false detections.

Re-examination of the misclassified change pixels revealed that the topographic effect, the primary reason of misclassification on the original Landsat images, was significantly reduced (Figs. 5–8). However, the minor changes over the sparsely treed areas may be the reason for low user's accuracy in post-correction change maps. For some changes pixels/patches, SVM assessed these areas as forest loss or regrowth. However, they appeared to be persisting sparse forest in the high resolution reference data. On the other hand, the Landsat reflectance values showed increased or decreased reflectance, indicating possible minor forest change. Thus the situation is ambiguous and depends in large part on the analyst. In this study, we treated such possible minor forest changes, which cannot be validated visually using the high resolution images, as a false detection. This potentially leads to a lower user's accuracy for the change classes (forest loss and regrowth). It is very difficult to validate such minor changes without examining ground records.

4.3. The impact of the terrain effect on change detection

Although the study sites were selected in mountainous areas, there are only a few steeply sloped regions (slopes > 30°), and the majority of the slopes were mild (5° < slope < 20°) (Fig. 10). The average angle of inclination ranged from 11° (Cherokee) to 13° (Uinta). The maximum angle of inclination ranged from 45° (Cherokee) to 55° (San Juan). Fig. 10 shows that the topographic effect on the Cherokee site is comparable to (or even slightly better than) other three study sites. This again verified our previous discussion that the Cherokee site represents the worst-case scenario among four study sites due to the combined effects of topography and phenology. However, the change detection result improved significantly after removing the topographic effect (Fig. 9b).

Fig. 11 shows the scatterplot of disagreement rate against angle of inclination. Disagreement rate here refers to the fraction of pixels

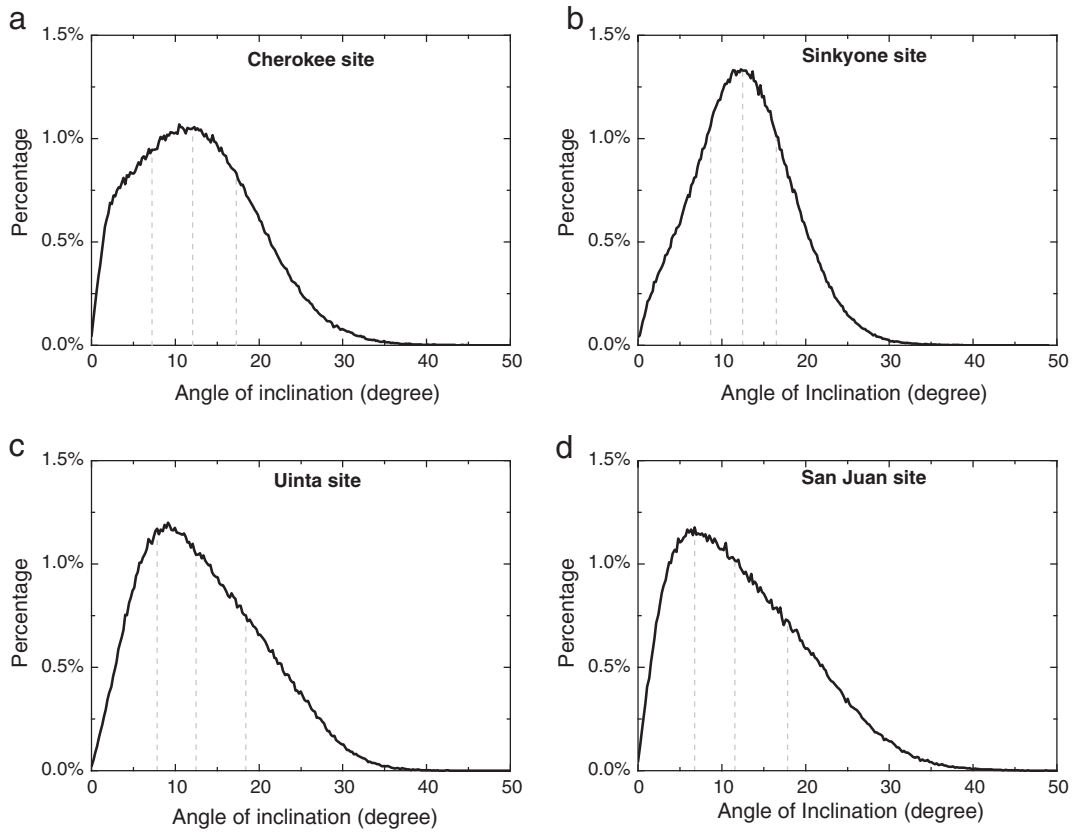


Fig. 10. Histogram of angle of inclination for four study sites. The quartiles are marked as three dashed lines.

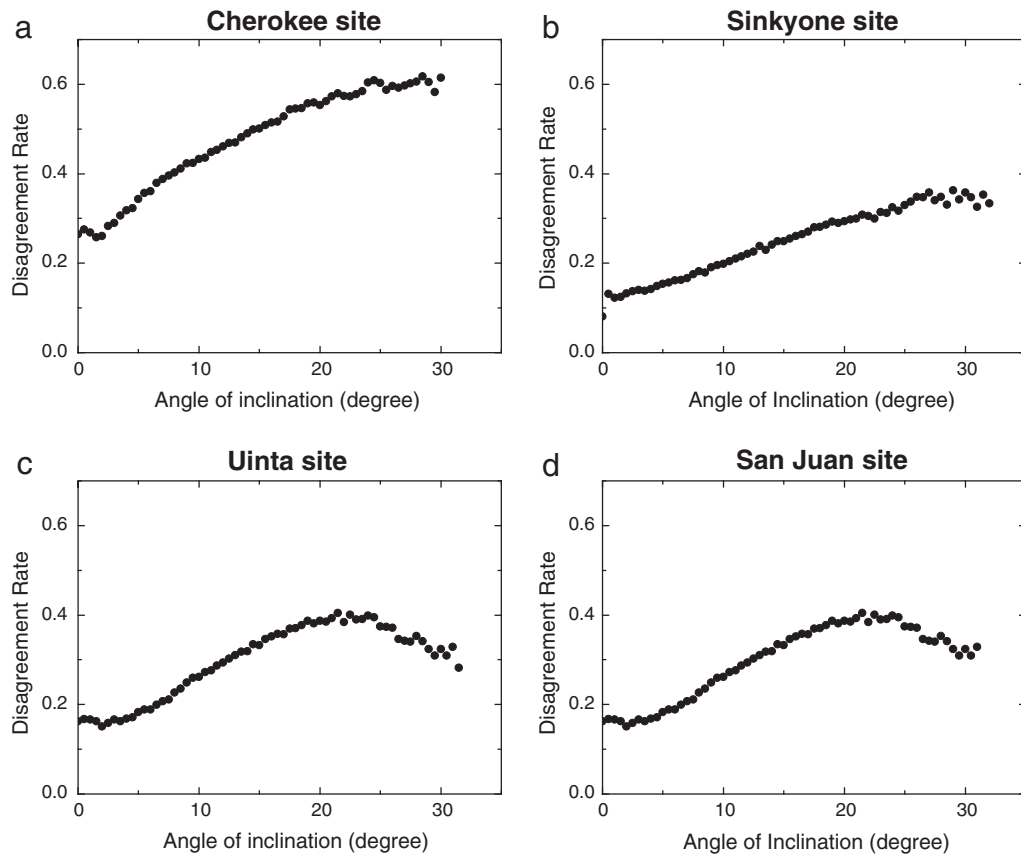


Fig. 11. Scatterplots of the disagreement rate against inclination angle over four study sites. The disagreement rate was calculated as the ratio of pixels in an inclination-angle interval (0.5° here), whose change-detection result changes after illumination correction.

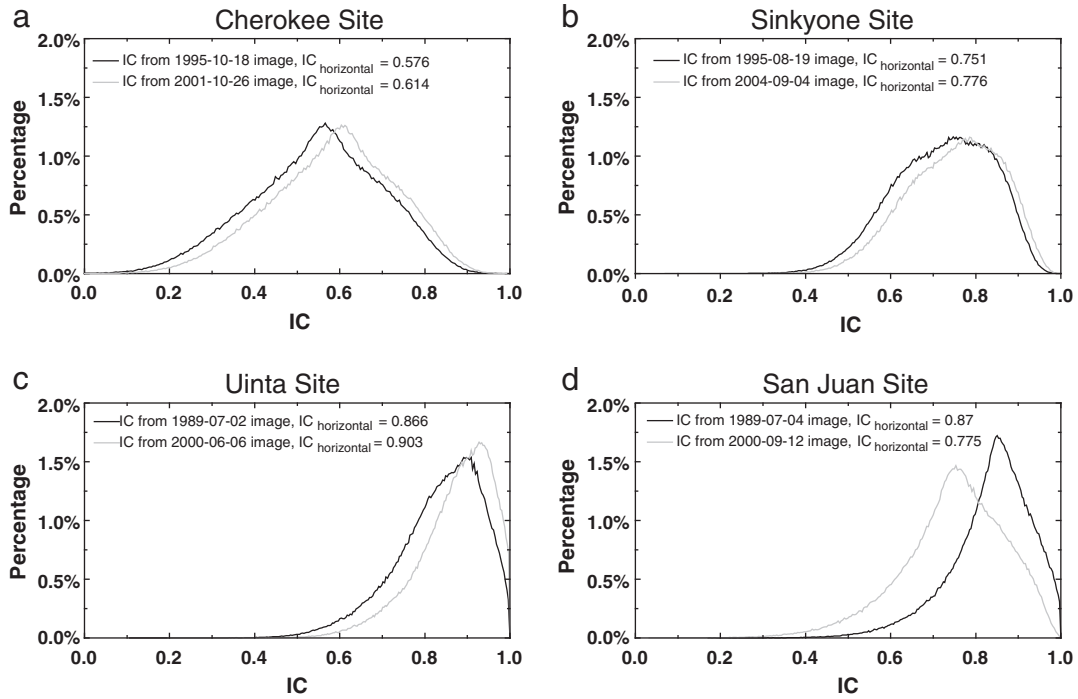


Fig. 12. Histogram of IC for four study sites.

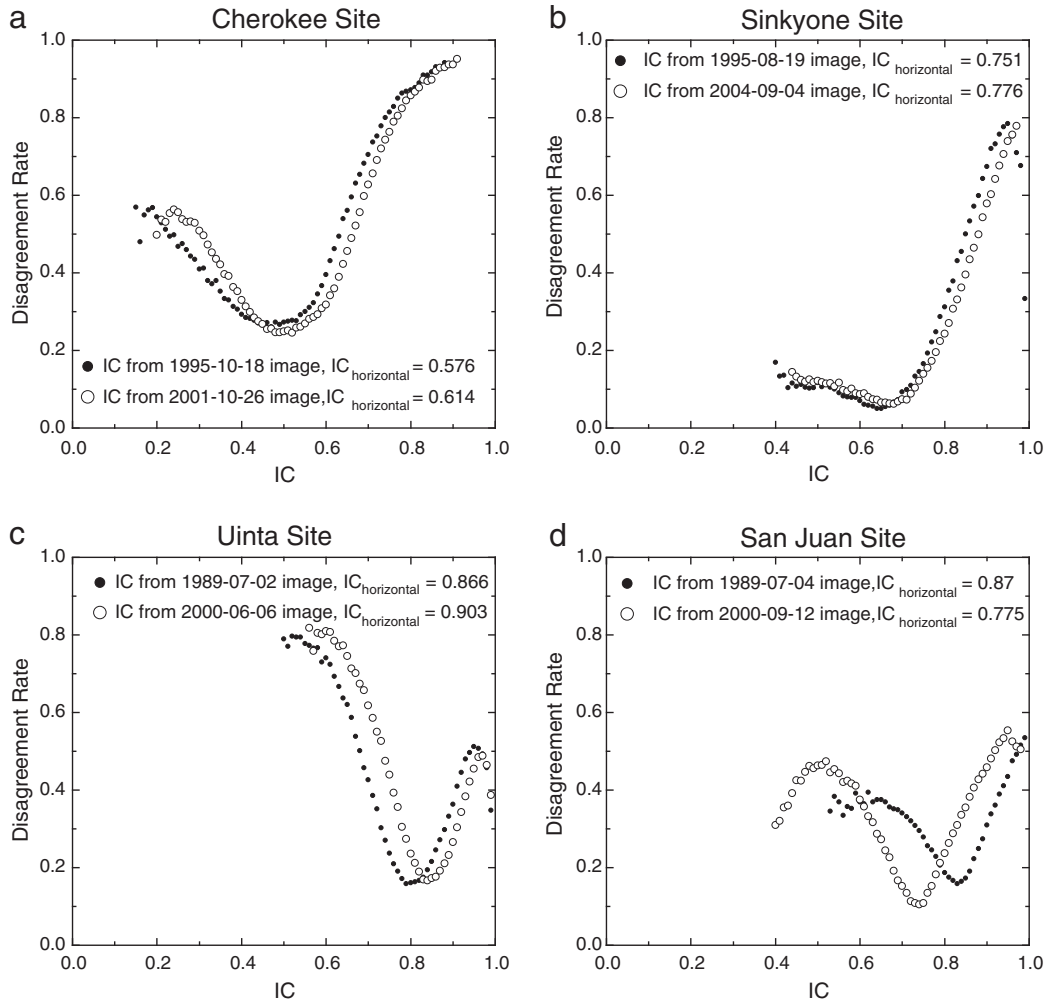


Fig. 13. Disagreement rate as a function of illumination condition (IC) over the four study sites. The definition of the disagreement rate is similar to that in Fig. 11. The only difference is that the IC interval is 0.005 here.

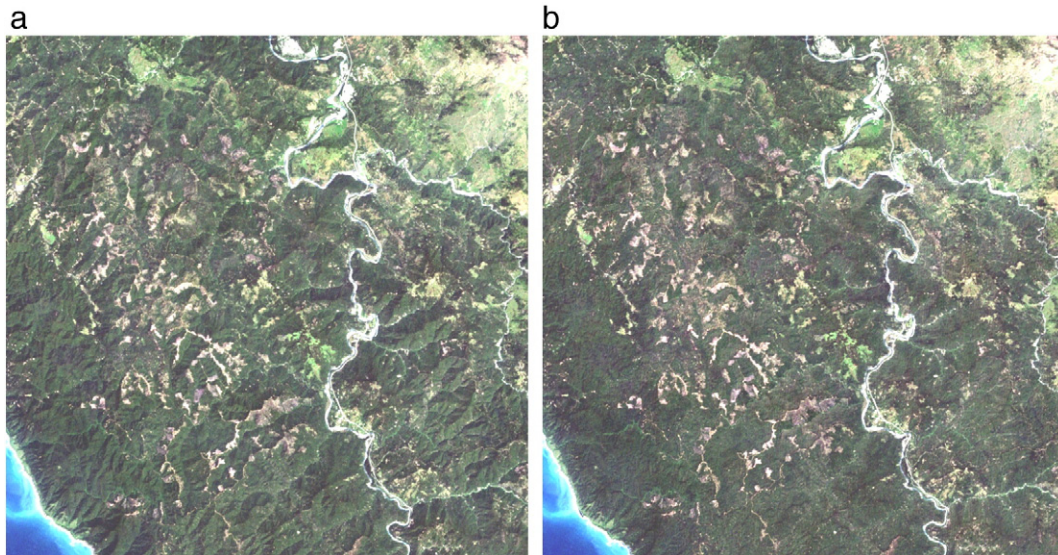


Fig. 14. The Landsat image acquired on May 13, 2003 over Sinkyone Wilderness State Park (WRS path 46 row 32). The panels a and b are original and corrected Landsat images, respectively. The images are true color images, whose RGB combination is Landsat bands 3, 2 and 1.

whose change detection result changed after the illumination correction. In each 0.5° bin, the pixels separated into two groups: those for which the change detection result changed after the illumination correction, and those for which illumination correction had no effect. The general tendency in all four study sites was for disagreement rate to increase with angle of inclination until the angle reaches 20 to 25° , after which the rate stays stable or decreases slightly. However, the rate of change varied among sites. The highest rate was observed on Cherokee site and the lowest rate on the Sinkyone site. For the Uinta and San Juan sites, the disagreement rate decreased slightly when the angle of inclination increased beyond about 22° . The lowest disagreement rate appeared at 1.5-, 1-, and 2-degree angles on Cherokee, Sinkyone, Uinta and San Juan site respectively.

Fig. 12 shows the histogram of IC for the Landsat image pairs for each site. There is a slightly mismatch, ranges from 0.01 to 0.03, between the peak value of the histogram and IC_H . Such a mismatch is corresponding to the peak, ranges from 7.5 to 11.4° , in the slope histograms (Fig. 10). For each study site, the shift between two IC histograms is primarily due to the different solar zenith angle from two acquisition dates. The difference of solar azimuth angles from two dates contributes marginally to the IC variance as shown in Eq. (4). The maximum histogram shift happens at San Juan site, from 0.85 to 0.75, corresponding to the longest time period between two acquisition dates of the year, July 4th–September 12th, among the four sites. Normally, longer intervals between acquisitions results in larger solar zenith angle changes, leading to larger variation in IC.

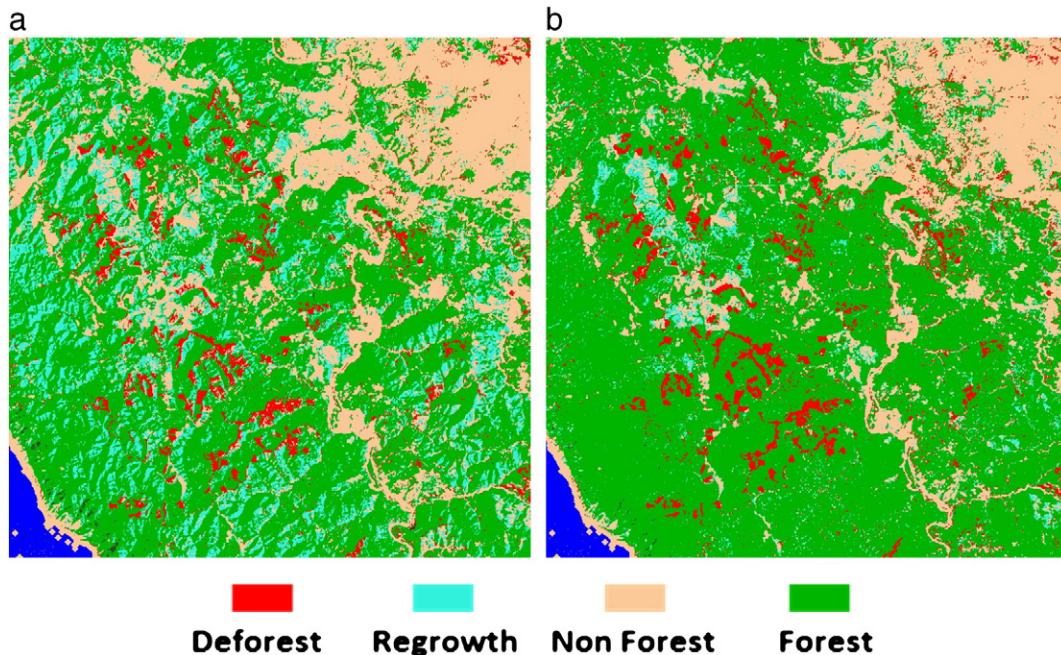


Fig. 15. Forest change maps from original (left) and illumination corrected (right) Landsat image pairs over Sinkyone site. The Landsat images were acquired on 1995-08-19 (Fig. 5a) and 2003-05-13 (Fig. 14a).

One exception is the Uinta site, whose acquisition dates were 26 days apart but showed a minimum IC peak shift, only 0.03. The acquisition dates for this site fell on two sides of the summer solstice (Jun 21), before which the solar zenith angle increases and decreases afterward. One acquisition date was 15 days before Jun 21, and the other was 11 days after Jun 21, comparable to a four-day interval in the normal situation. Fig. 13 shows the relationship between disagreement rate and IC. There are two curves in each plot, corresponding to the IC maps for the Landsat imagery pair on each study site. For all eight curves over four study sites, the disagreement rate decreased with increasing IC and reached the lowest rate as IC approached IC_H . It is interesting that the lowest rate did not coincide exactly with IC_H ; this was because the training data were re-selected through TDA procedure after illumination correction. With a new training set, the classification result on a horizontal surface might change although the reflectance does not change after illumination correction. Beyond this value the disagreement rate increased with increasing IC. The curves within each study site were similar, but the curves from different sites vary significantly. On the Cherokee and Sinkyone sites, the highest disagreement rate occurred at the end of the right tail of the curve, where $IC > IC_H$. This means the most significant disagreement happened at the slopes that became brighter due to the topographic effect. In contrast, the highest disagreement on the Uinta site happened at the end of the left tail of the curve, where $IC < IC_H$. This indicates that the most significant disagreement happened at the slopes that became darker due to the topographic effect. For the San Juan site, the right and left tail of the curve reach a similar level of disagreement rate. The relationship between disagreement rate and IC is the result of a combination effect of terrain conditions, sun locations and the forest BRDF.

It is not always possible to find images with close acquisition date of year due to clouds and/or data availability. When the images are from different season, will the different incident angle, longer shadows and different shadow angles compromise the performance of the illumination correction algorithm? In addition to the studies on same season image pairs, we applied the illumination correction and change detection algorithms on a pair of Landsat images from different season over Sinkyone site. A Landsat image acquired on May 13, 2003 in spring (Fig. 14) is used together with the image acquired on Aug 19, 1995 in summer (Fig. 5 upper panels) to retrieve the forest changes. The mean IC of the spring image is 0.84, while the mean IC for summer image is 0.72. The IC difference of these two images is much greater than it between two summer images, which are 0.72 and 0.75 respectively (Table 1). In such a situation, the performance of the illumination correction algorithm plays a greater role on the change detection accuracy. Fig. 15 shows the forest change detection result from spring and summer images. The change detection on the uncorrected Landsat data overestimates the regrowth (Fig. 15a), similar to the result from two summer images (Fig. 9c). After illumination correction, the change detection accuracy got significantly improved (Fig. 15b). This improvement, again, is comparable to the improvement achieved from two corrected summer images (Fig. 9d).

4.4. Future research

Correction for topographic illumination should be considered in forest change detection algorithms as a standard pre-processing step, especially in mountainous areas. In order to assess IC on classification of non-forest land cover types, it would be useful to assess the performance of this new algorithm on more study sites and, if needed, refine it to suit different land cover types. One interesting topic to investigate is the relationship between the disagreement rate and IC. Research in this area could help to better understand the implications of the topographic effect for product accuracy, which is actually a combined effect from multiple factors. Another research topic is to compare the improvements on atmospheric corrected and uncorrected

Landsat images. It will be useful to quantitatively assess the product accuracy improvements due to the combination of atmospheric correction and IC over different land cover types and terrain conditions. Finally, it is desired to examine the dependence of the improvement in change detection on classification methodology. All topics eventually will contribute to more accurate illumination correction models and image classification algorithms.

5. Conclusions

Although Landsat data are widely used for monitoring forest change, the accuracy of change detection results drops greatly in mountainous areas because of topographic illumination artifacts. We developed an illumination correction algorithm and produced a set forest change maps from both original and corrected Landsat images. Validation over four study sites indicated a significant overall accuracy improvement, over 10%, for the change detection results after the illumination correction. In the Cherokee site, which was affected by phenology as well as topography, overall accuracy improved 24%.

It was found that the disagreement rates between the original and corrected Landsat based change maps increases as the ground inclination angle increasing. With IC increasing, the disagreement rate decreases first then increases. The lowest disagreement rate occurred when IC is close to IC_H , but not exactly at IC_H in our study cases.

Acknowledgment

Support for this research was provided by the NASA Terrestrial Ecology Program and the NASA MEASURES Program. Thanks for three reviewers' useful and constructive comments. USDA is an equal opportunity provider and employer.

References

- Band, L. E. (1993). Effect of land surface representation on forest water and carbon budgets. *Journal of Hydrology*, 150, 749–772.
- Bowcutt, F. (1996). A floristic study of Sinkyone Wilderness State Park, Mendocino County, California. *The Wasmann Journal of Biology*, 51, 64–143.
- Burges, C. J. C. (1998). A tutorial on support vector machines for pattern recognition. *Data Mining and Knowledge Discovery*, 2, 121–167.
- Congalton, R. G., & Mead, R. A. (1983). A quantitative method to test for consistency and correctness in photo interpretation. *Photogrammetric Engineering and Remote Sensing*, 49, 69–74.
- DeVelice, R. L., Ludwig, J. A., Moir, W. H., & Ronco, F., Jr. (1986). A classification of forest habitat types of northern New Mexico and southern Colorado. *USDA Forest Service General Technical Report RM-GTR-131, Rocky Mountain Forest and Range Experiment Station, Fort Collins, Colorado, USA*.
- Duguay, C. R., & LeDrew, E. F. (1992). Estimating surface reflectance and albedo from Landsat-5 TM over rugged terrain. *Photogrammetric Engineering and Remote Sensing*, 58, 551–558.
- Ekstrand, Sam (1996). Landsat TM-based forest damage assessment: Correction for topographic effects. *Photogrammetric Engineering and Remote Sensing*, 62, 151–161.
- Floyd-Hanna, L., Spencer, A. W., & Romme, W. H. (1996). Biotic communities of the semiarid foothills and valleys. In R. Blair (Ed.), *The western San Juan Mountains: Their geology, ecology, and human history* (pp. 143–158). Niwot, Colorado, USA: University Press of Colorado.
- Foody, G. M., & Mathur, A. (2004). A relative evaluation of multiclass image classification by support vector machines. *IEEE Transactions on Geoscience and Remote Sensing*, 42, 1335–1343.
- Holben, B., & Justice, C. (1980). The topographic effect on spectral response from nadir pointing sources. *Photogrammetric Engineering and Remote Sensing*, 46, 1191–1200.
- Huang, C., Davis, L. S., & Townshend, J. R. G. (2002). An assessment of support vector machines for land cover classification. *International Journal of Remote Sensing*, 23, 725–749.
- Huang, C., Davis, L. S., & Townshend, J. R. G. (2010a). An assessment of support vector machines for land cover classification. *International Journal of Remote Sensing*, 23, 725–749.
- Huang, C., Goward, S. N., Masek, J. G., Thomas, N., Zhu, Z., & Vogelmann, J. E. (2010b). An automated approach for reconstructing recent forest disturbance history using dense Landsat time series stacks. *Remote Sensing of Environment*, 114, 183–198.
- Huang, C., Song, K., Kim, S., Townshend, J. R. G., Davis, P., Masek, J., et al. (2008). Use of a dark object concept and support vector machines to automate forest cover change analysis. *Remote Sensing of Environment*, 112, 970–985.
- Masek, J. G., Goward, S., Cohen, W., Wolfe, R., Huang, C., & Hall, F. (2007). Assessing North American forest disturbance from the Landsat archive. *IGARSS 2007: International Geoscience and Remote Sensing Symposium* (pp. 5294–5297).

- Masek, J. G., Huang, C., Wolfe, R., Cohen, W., Hall, F., Kutler, J., et al. (2008). North American forest disturbance mapped from a decadal Landsat record. *Remote Sensing of Environment*, 112, 2914–2926.
- Masek, J. G., Vermote, E. F., Saleous, N. E., Wolfe, R., Hall, F. G., Huemmrich, K. F., et al. (2006). A Landsat surface reflectance dataset for North America, 1990–2000. *IEEE Geoscience and Remote Sensing Letters*, 3, 68–72.
- Mauk, R., & Henderson, J. (1984). Coniferous forest habitat types of northern Utah. *USDA Forest Service, Intermountain Forest and Range Experiment Station, General Technical Report INT-170* (pp. 88–89).
- Meyer, P., Itten, K. I., Kellenbenberger, T., Sandmeier, S., & Sandmeier, R. (1993). Radiometric corrections of topographically induced effects on Landsat TM data in an alpine environment. *ISPRS Journal of Photogrammetry and Remote Sensing*, 48, 17–28.
- Pandey, D. N. (2002). Sustainability science for tropical forests. *Conservation Ecology*, 6, 13.
- Riano, D., Chuvieco, E., Salas, J., & Aguado, I. (2003). Assessment of difference topographic corrections in Landsat-TM data for mapping vegetation types. *IEEE Transactions on Geoscience and Remote Sensing*, 41, 1056–1061.
- Sadeq, H., Drummond, J., & Li, Z. (2012). Evaluation of ASTER GDEM v. 2 using GPS checkpoints, OSGB DEM values and photogrammetrically derived DEMs. *International Archives of the Photogrammetry, Remote Sensing and Spatial, Information Sciences, XXXIX-B4* (pp. 295–300).
- Shephard, J. D., & Dymond, J. R. (2003). Correcting satellite imagery for the variance of reflectance and illumination with topography. *International Journal of Remote Sensing*, 24, 3505–3514.
- Stehman, S. V., & Czaplewski, R. L. (1998). Design and analysis for thematic map accuracy assessment: Fundamental principles. *Remote Sensing of Environment*, 64, 331–344.
- Tan, B., Wolfe, R., Masek, J. G., Gao, F., & Vermote, E. F. (2010). An illumination correction algorithm on Landsat-TM data. *IGARSS 2010: International Geoscience and Remote Sensing Symposium* (pp. 1964–1967).
- Teillet, P. M., Guindon, B., & Goodenough, D. G. (1982). On the slope-aspect correction of multispectral scanner data. *Canadian Journal of Remote Sensing*, 8, 84–106.
- Townshend, J. R., Masek, J. G., Huang, C., Vermote, E. F., Gao, F., Channan, S., et al. (2012). Global characterization and monitoring of forest cover using Landsat data: Opportunities and challenges. *International Journal of Digital Earth*, 5, 373–397.
- Vermote, E. F., El Saleous, N., Justice, C. O., Kaufman, Y. J., Privette, J. L., Remer, L., et al. (1997). Atmospheric correction of visible to middle-infrared EOS-MODIS data over land surfaces: Background, operational algorithm and validation. *Journal of Geophysical Research*, 102, 17131–17141.
- Vicente-Serrano, S. M., Perez-Cabello, F., & Lasanta, T. (2008). Assessment of radiometric correction techniques in analyzing vegetation variability and change using time series of Landsat images. *Remote Sensing of Environment*, 112, 3916–3934.
- Whitted, T. (1979). An improved illumination model for shaded display. *Proceedings of the 6th Annual Conference on Computer Graphics and Interactive Technique* (pp. 343–349).
- Wolfe, R., Masek, J., Saleous, N., & Hall, F. (2004). LEDAPS: Mapping North American disturbance from the Landsat record. *IGARSS 2004: International Geoscience and Remote Sensing Symposium* (pp. 1–4).
- Yoke, K. A., & Rennie, J. C. (1996). Landscape ecosystem classification in the Cherokee National Forest, East Tennessee, U.S.A. *Environmental Monitoring and Assessment*, 39, 323–338.
- Zhu, G., & Blumberg, D. G. (2002). Classification using ASTER data and SVM algorithm: The case study of Beer Sheva, Israel. *Remote Sensing of Environment*, 80, 233–240.